

## Geometric Registration Based on Distortion Estimation

Wei Zeng

Florida International University

wzeng@cs.fiu.edu

Feng Luo

Rutgers University

fluo@math.rutgers.edu

Mayank Goswami

Max-Planck Institute for Informatics

gmayank@mpi-inf.mpg.de

Xianfeng Gu

Stony Brook University

gu@cs.stonybrook.edu

### Abstract

*Surface registration plays a fundamental role in many applications in computer vision and aims at finding a one-to-one correspondence between surfaces. Conformal mapping based surface registration methods conformally map 2D/3D surfaces onto 2D canonical domains and perform the matching on the 2D plane. This registration framework reduces dimensionality, and the result is intrinsic to Riemannian metric and invariant under isometric deformation. However, conformal mapping will be affected by inconsistent boundaries and non-isometric deformations of surfaces. In this work, we quantify the effects of boundary variation and non-isometric deformation to conformal mappings, and give the theoretical upper bounds for the distortions of conformal mappings under these two factors. Besides giving the thorough theoretical proofs of the theorems, we verified them by concrete experiments using 3D human facial scans with dynamic expressions and varying boundaries. Furthermore, we used the distortion estimates for reducing search range in feature matching of surface registration applications. The experimental results are consistent with the theoretical predictions and also demonstrate the performance improvements in feature tracking.*

### 1. Introduction

As a consequence of the fast development of 3D scanning technologies, a large number of 3D databases are generated. Accordingly, fast and automatic processing techniques for such databases are greatly desired. 3D surface registration is a fundamental tool, which aims at finding a mapping (one-to-one correspondence) between two 3D surfaces. 3D surface tracking requires generating the mappings over a series of surface frames in 3D spatial-temporal data (3D geometry video or 4D data). Registration is a key component of the solution to the tracking issue.

Surface registration and tracking has a broad range of applications in many engineering and medical fields [22, 4, 19, 15, 8, 16, 7, 11, 18], such as shape matching, classification, and recognition for deformable objects in computer vision, shape space construction in geometric modeling, morphological study and data fusion in medical imaging, shape mapping or animation in game/film industry, and so on. In the last decade, many 3D surface registration methods have been developed. The most well-known iterative closest point (ICP) method [2] works well for rigid motions but cannot handle the nonrigid deformation and inconsistent boundary problems. Most existing methods directly deal with nonrigid deformations in  $\mathbb{R}^3$ , but always stop at a local optima and hardly get a global solution.

Surface conformal mapping based methods have been developed for surface matching [17, 6, 12], registration [3, 25, 26], and tracking [27]. The key idea is to map surfaces to 2D canonical domains and then solve the surface registration problem as an image registration problem. The conformal mapping based methods can handle nonrigid deformations and generate diffeomorphisms between surfaces. Surface conformal mapping can be generalized to surface quasiconformal mapping, which has great potential to handle large-scale nonrigid (including non-isometric) deformations in surface registration application [24, 13, 14].

**Main Problem.** Although conformal mapping based surface registration framework reduces the dimension of the search space, is intrinsic to the Riemannian metric and invariant under rigid motion, preserves symmetry, and ensures the mapping to be diffeomorphic, it depends on the boundary variations and the non-isometric distortion from physical deformations of the input surface. The fundamental questions to be addressed in this work are as follows:

*How to quantify the effects of boundary variation and non-isometric deformation to the conformal mapping? How sensitive is the conformal mapping based registration method to boundary variation and non-isometric deformation?*

Today's 3D scanning technique is able to offer high resolution, high accuracy, and high speed 3D geometric surface data. For example, the 3D camera in [21] can capture dynamic facial expression at 30 frames per second, with 3 millions samples per frame, and with 0.2 mm depth accuracy. Due to the high scanning speed, we expect the distortions caused by the expression change between two adjacent frames are very small. Furthermore, the variations of the boundary cluttering caused by the head rotation between two adjacent frames are small as well. Therefore, when we map two adjacent frames onto the unit disk by conformal mappings, the deviation of the two images of the same point on the face surface is expected to be small. It is highly desirable to quantify the deviation on conformal mapping in terms of both boundary variation and non-isometric deformation. Furthermore, once we have the distortion estimation of conformal maps, we can reduce the search range for matching the feature points of two surfaces, which will improve the efficiency and accuracy of surface registration.

This work presents upper bound estimation on distortions of conformal maps caused by surface boundary variations and non-isometric deformations. These theoretical results are not classical, and to the best of our knowledge, this is the first work to give rigorous theoretical upper bound estimation on distortion of conformal maps in the above cases.

**Our Solution.** The framework of surface registration based on conformal mapping is as follows. Suppose we want to register two surfaces, source  $S_1$  and target  $S_2$ , namely, to find a map  $\phi : S_1 \rightarrow S_2$ . First we conformally map both of them to the unit disk  $\phi_k : S_k \rightarrow \mathbb{D}, k = 1, 2$ . If we can find a mapping between these two planar images  $\tilde{\phi} : \mathbb{D} \rightarrow \mathbb{D}$ , then the registration can be obtained as  $\phi = \phi_2^{-1} \circ \tilde{\phi} \circ \phi_1$ .

Suppose  $S_1$  and  $S_2$  are two scans of the same human face with different viewing angles. Then their boundaries will be inconsistent. Let  $\Omega$  be the common region of them,  $\Omega = S_1 \cap S_2$ , and  $\Gamma = \partial\Omega$  be its boundary. Then we use the furthest distance of each point on  $\phi_k(\Gamma)$  to the unit circle to represent the boundary inconsistency, namely,

$$\varepsilon_k := \max_{p \in \Gamma} 1 - |\phi_k(p)|, k = 1, 2.$$

If  $\varepsilon_k$ 's are zeros, then two surfaces have the same boundary. *Furthermore*, assume the face surfaces are with expression change, which is a nonrigid deformation. Intuitively, if the mapping between the two surfaces is conformal (the deformation is isometric), then it maps infinitesimal circles on the source to infinitesimal circles on the target; if it is quasiconformal (the deformation is non-isometric), then it maps infinitesimal circles to infinitesimal ellipses. We use a complex function, the so-called Beltrami coefficient  $\mu$ , to indicate the shape of ellipses (see Fig. 1). The argument of  $\mu$  gives the orientation of the ellipse, the magnitude of  $\mu$  gives the eccentricity of the ellipse, and the ratio between the longer axis and the shorter axis of the ellipse is

$(1 + |\mu|)/(1 - |\mu|)$ . The *angle distortion*  $K$  of a quasiconformal map is defined as

$$K = \|\mu\|_\infty := \max_{p \in S_1} |\mu(p)|.$$

Any homeomorphism between two compact surfaces must be quasiconformal. Conformal map is a special case of quasiconformal map whose  $\mu$  is zero everywhere.

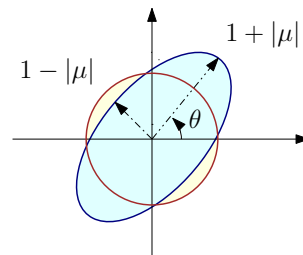


Figure 1. Geometric illustration of quasiconformal mapping.

Our task is to estimate the upper bound of the differences between two images of the same point  $p \in \Omega$  in terms of both boundary variations  $\varepsilon_1, \varepsilon_2$  and the angle distortion  $K$ ,

$$|\phi_1(p) - \phi_2(p)| < g(\varepsilon_1, \varepsilon_2, K), \forall p \in \Omega.$$

By applying geometric methods from *quasiconformal geometry* and *harmonic analysis*, we give the explicit upper bound  $g(\varepsilon_1, \varepsilon_2, K)$ , which is a linear function of both  $\varepsilon_k$ 's and  $K$  (see Theorems 3.1, 3.2, and 3.3 of this work).

**Contribution.** In this work, we estimate the distortions of conformal mappings both theoretically and experimentally. We present three main theorems, along with rigorous proofs based on quasiconformal geometry, which state the upper bounds of distortion with respect to the boundary variation and non-isometric deformation. We then utilize the distortion bound for feature registration purposes. The search range is reduced to a smaller, local neighborhood, thereby reducing the complexity of search greatly. The contributions of this work can be summarized as follows:

1. Quantify the distortion of conformal mappings caused by boundary variation.
2. Quantify the distortion of conformal mappings caused by non-isometric deformations.
3. Present a registration algorithm which searches corresponding features in the given distortion range.

## 2. Theoretical Background

In this section, we briefly introduce the most related theoretical background. For a comprehensive treatment and the extensive literature on the subject one may refer to [1].

## 2.1. Quasiconformal Geometry

Suppose  $f(z) : \mathbb{C} \rightarrow \mathbb{C}$  is a complex valued function on the complex plane, and its representation is  $f(x + iy) = u(x, y) + iv(x, y)$ ,  $z = x + iy$ . Assume  $f$  is differentiable. The complex differential operators are defined as

$$\frac{\partial}{\partial z} = \frac{1}{2} \left( \frac{\partial}{\partial x} - i \frac{\partial}{\partial y} \right), \quad \frac{\partial}{\partial \bar{z}} = \frac{1}{2} \left( \frac{\partial}{\partial x} + i \frac{\partial}{\partial y} \right).$$

The *Beltrami equation* is

$$\frac{\partial f}{\partial \bar{z}} = \mu \frac{\partial f}{\partial z}, \quad (1)$$

where  $\mu$  is called the *Beltrami coefficient*,  $\|\mu\|_\infty < 1$ .  $f(z)$  is conformal if and only if  $\frac{\partial f}{\partial \bar{z}} = 0$ , i.e.,  $\mu = 0$ .  $f(z)$  is *quasiconformal* if it satisfies Eqn. (1). The quasiconformal mapping is uniquely determined by  $\mu$  up to a conformal transformation, which is stated in the classical measurable Riemann mapping theorem [1].

**Theorem 2.1 (Measurable Riemann Mapping)** *Suppose  $S \subset \mathbb{C}$  is a compact simply connected domain with a smooth boundary. Suppose  $\mu : S \rightarrow \mathbb{C}$  is a measurable complex function, such that  $\|\mu\|_\infty < 1$ . Then there exists a quasiconformal homeomorphism  $f : \Omega \rightarrow \mathbb{D}$ , whose Beltrami coefficient is  $\mu$ . It is unique up to a Möbius transformation.*

Namely, the space of quasiconformal homeomorphism (QCH) between  $\Omega$  and  $\mathbb{D}$  and the functional space of Beltrami coefficients have the following relation

$$QCH(S, \mathbb{D}) / \{\text{Möbius}\} \cong \{\mu | \mu : S \rightarrow \mathbb{C}, \|\mu\|_\infty < 1\}.$$

## 2.2. Surface Ricci Flow

*Ricci flow* refers to the process of deforming Riemannian metric  $\mathbf{g}$  proportionally to the Gauss curvature  $K$ , such that the curvature evolves according to a heat diffusion process and eventually becomes constant everywhere. Analytically, surface Ricci flow is defined as  $\frac{d\mathbf{g}}{dt} = -2K\mathbf{g}$ . It conformally deforms the Riemannian metric and converges to constant curvature metric [5, 10]. This shows the following uniformization theorem:

**Theorem 2.2 (Uniformization)** *Suppose  $S$  is a closed, compact Riemannian surface. Then, depending on the topology of  $S$ , it can be conformally deformed to one of three canonical shapes: the unit sphere  $\mathbb{S}^2$ , the flat torus  $\mathbb{R}^2/\Gamma$  ( $\Gamma$  is a subgroup of Euclidean translation), or  $\mathbb{H}^2/\Gamma$  ( $\Gamma$  is a subgroup of hyperbolic rigid motion group).*

This shows that for surfaces with Riemannian metrics, we can find a conformal atlas  $\{(U_\alpha, \phi_\alpha)\}$ , such that all the chart transitions  $\phi_{\alpha\beta} : \phi_\alpha(U_\alpha \cap U_\beta) \rightarrow \phi_\beta(U_\alpha \cap U_\beta)$  are the elements in  $\Gamma$ , which are planar conformal mappings.

## 2.3. Auxiliary Metric

Here we give a constructive method to solve the Beltrami equation, namely, to recover the mapping from its Beltrami coefficient. Suppose  $\phi : \Omega \rightarrow \mathbb{D}$ ,  $\Omega$  is in the  $z$ -plane,  $\mathbb{D}$  is in the  $w$ -plane. Then

$$dw(z) = \frac{\partial w(z)}{\partial z} dz + \frac{\partial w(z)}{\partial \bar{z}} d\bar{z} = w_z(dz + \mu d\bar{z}).$$

The pullback metric induced by  $\phi$  on  $\Omega$  is

$$\phi^* |dw|^2 = |w_z|^2 |dz + \mu d\bar{z}|^2,$$

therefore, the pullback metric is conformal to the *auxiliary metric*  $|dz + \mu d\bar{z}|^2$ . We have the following theorem:

**Theorem 2.3 (Auxiliary Metric)** *A quasiconformal mapping associated with Beltrami coefficient  $\mu$  becomes a conformal mapping under the auxiliary metric,*

$$\begin{aligned} \phi : (\Omega, |dz|^2, \mu) &\rightarrow (\mathbb{D}, |dw|^2) \equiv \\ &\phi : (\Omega, |dz + \mu d\bar{z}|^2) \rightarrow (\mathbb{D}, |dw|^2). \end{aligned}$$

## 3. Distortion Estimation Theorems

This section introduces the main theorems of this work. We use concepts from *harmonic measure* [9] and *quasiconformal geometry* [1] to obtain the distortion bounds.

### 3.1. Boundary Variation

We first estimate the distortion arising due to inconsistent boundaries. The conformal mappings of the scanned static faces might be almost identical except that their boundaries do not really match. One then needs to estimate how much the conformal mapping of one surface differs from another. We provide two estimates. In the first case the boundary of one surface is contained in the other. Using this, we solve the second case in which the boundaries possibly intersect.

#### 3.1.1 Boundary Containment

Let  $A_\varepsilon$  denote the open annulus  $A_\varepsilon = \{z \in \mathbb{D} : 1 - \varepsilon < |z| < 1, 0 < \varepsilon < 1\}$ . Let  $\Gamma$  be a smooth curve embedded in  $A_\varepsilon$  and  $\Omega$  be the interior of  $\Gamma$ . Furthermore, let  $\Gamma$  be *star-shaped* with respect to the origin  $O$ , meaning that for all  $z \in \Gamma$ , the line joining  $O$  to  $z$  is contained inside  $\Omega$  (similar to Fig. 2).

Let  $\phi : \Omega \rightarrow \mathbb{D}$  be the Riemann mapping which fixes the origin and (the continuous extension of  $\phi$  to the boundary of  $\Omega$ ) maps the point  $p = \Gamma \cap \mathbb{R}^+$  (note that star-shaped property of  $\Gamma$  implies uniqueness of  $p$ ) to the point 1. Let  $z \in \Omega$ . We are interested in estimating  $|\phi(z)| - |z|$  and  $|\arg(\phi(z)) - \arg(z)|$ . For this case, we have

**Theorem 3.1 (Distortion for Boundary Containment)**

*Let  $\Omega$ ,  $\phi$ , and  $\varepsilon$  be as above. Then,  $\forall z \in \Omega$ ,*

1. [Magnitude Distortion]:

$$|\phi(z)| - |z| < \varepsilon,$$

2. [Argument Distortion]:

$$|\arg(\phi(z)) - \arg(z)| \leq 2\varepsilon + O(\varepsilon^2).$$

The proof is based on harmonic measure and its invariance under conformal changes. The mathematical proofs of both assertions are provided in the supplementary material.

### 3.1.2 Boundary Intersection

We consider two surfaces with a considerable overlapping region and inconsistent boundaries, as shown in Fig. 2.

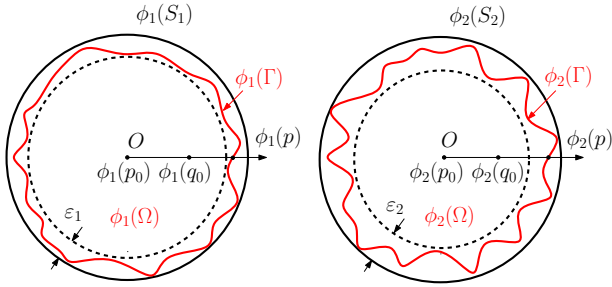


Figure 2. Distortion estimation of conformal mappings between two surfaces  $S_1, S_2$  with big overlapping region  $\Omega$ .

We first briefly describe the setting and the hypothesis. Let  $S_1$  and  $S_2$  be two simply connected Riemann surfaces embedded in  $\mathbb{R}^3$ . Assume that they have a big overlapping region,  $\Omega = S_1 \cap S_2$ , which is simply connected. Let  $\Gamma$  be the boundary of  $\Omega$ . Fix  $p_0$  and  $q_0$  in  $\Omega$  as base points. Suppose  $S_1$  and  $S_2$  are conformally mapped to the unit disk. Let  $\phi_k : S_k \rightarrow \mathbb{D}$  denote the corresponding Riemann mappings, with the normalization conditions

1.  $\phi_1(p_0) = 0$  and  $\phi_2(p_0) = 0$ .
2.  $\phi_1(q_0) \in \mathbb{R}^+$  and  $\phi_2(q_0) \in \mathbb{R}^+$ .

Furthermore, for all points  $p \in \Gamma$ ,  $|\phi_1(p)| > 1 - \varepsilon_1$  and  $|\phi_2(p)| > 1 - \varepsilon_2$ ,  $0 < \varepsilon_1, \varepsilon_2 < 1$ . Also, both  $\phi_1(\Gamma)$  and  $\phi_2(\Gamma)$  are star-shaped (with respect to the origin) Jordan curves.

We are now in a position to state our theorem as follows:

### Theorem 3.2 (Distortion for Boundary Intersection)

With the above hypothesis,  $\forall z \in \Omega$ ,

1. [Magnitude Distortion]:

$$||\phi_1(z)| - |\phi_2(z)|| < \varepsilon_1 + \varepsilon_2,$$

2. [Argument Distortion]:

$$|\arg \phi_1(z) - \arg \phi_2(z)| < 2\varepsilon_1 + 2\varepsilon_2 + O(\varepsilon_1^2 + \varepsilon_2^2).$$

This theorem is proved based on Theorem 3.1. Details can be found in the supplementary material.

## 3.2. Non-isometric Deformation

We then estimate the magnitude and argument changes for a point inside a domain under the action of a quasiconformal map, usually induced by a non-isometric deformation. As previously mentioned, quasiconformal maps intuitively distort angles by a bounded amount. This distortion is encoded in the Beltrami coefficient  $\mu$  of the map. By the Riemann mapping theorem, all simply connected domains are conformally equivalent to the unit disk  $\mathbb{D}$ . without loss of generality, we just study the distortion caused by a quasiconformal mapping on the unit disk.

Assume that all quasiconformal mappings  $f : \mathbb{D} \rightarrow \mathbb{D}$  are normalized, i.e.,  $f(0) = 0, f(1) = 1$ . Further, let  $\mu(z) = \frac{f_{\bar{z}}}{f_z}$  be the Beltrami coefficient of  $f$ , with  $\|\mu\|_\infty \leq K < 1$ . We have the following theorem:

### Theorem 3.3 (Distortion for Non-isometric Deformation)

Let  $f$ , and  $\mu$  be as above. Then

$$|f(z) - z| \leq 13 \cdot \|\mu\|_\infty, \forall |z| \leq 1.$$

The distortion estimation is based on the deformation theorem for quasiconformal mappings [1]. Intuitively, a one parameter family of mappings,  $h(t, z)$  with Beltrami coefficient  $t\mu$ , is constructed, such that  $h(0, z)$  is the identity map, and  $h(1, z) = f(z)$ . The deformation velocity field is  $V(t, z) = \frac{d}{dt}h(t, z)$ , which has an explicit form involving integrating the Cauchy kernel  $1/(w - z)$ . The bound of the deformation velocity field  $|V(t, z)|$  can be estimated, whose integration along  $t$  gives the bound of the distortion  $|h(1, z) - h(0, z)|$ , namely,  $|f(z) - z|$ . The mathematical proof can be found in the supplementary material.

## 4. Algorithm

In this section, we will explain the computational algorithms. The surfaces are approximated by piecewise linear triangle meshes,  $M = (V, E, F)$ , where  $V, E, F$  represent the vertex, edge and face sets of the mesh, respectively.

### 4.1. Conformal Mapping Using Ricci Flow

We define the discrete Gauss curvature as angle deficit at each vertex,

$$K(v_i) = \begin{cases} 2\pi - \sum_{jk} \theta_{jk}^i, & v_i \notin \partial M \\ \pi - \sum_{jk} \theta_{jk}^i, & v_i \in \partial M \end{cases},$$

where  $\theta_{jk}^i$  is the corner angle in triangle  $[v_i, v_j, v_k]$  at  $v_i$ . The discrete conformal factor is defined as a function  $\lambda : V \rightarrow \mathbb{R}$ . The discrete Riemannian metric is represented as the edge length,  $l_{ij} = e^{\lambda_i + \lambda_j} l_{ij}^0$ , where  $l_{ij}^0$  is the initial edge length. Let  $\bar{K}(v_i)$  be the target curvature. Then the discrete surface Ricci flow is given by

$$\frac{d\lambda_i}{dt} = \bar{K}_i - K_i,$$

with the constraint  $\sum_i \lambda_i = 0$ . This is equivalent to the negative gradient flow of a convex energy  $\int \sum_i (\bar{K}_i - K_i) d\lambda_i$ , which can be optimized more efficiently using Newton’s method. Details can be found in [25].

## 4.2. Quasiconformal Mapping by Auxiliary Metric

We apply the quasiconformal mapping algorithm based on the auxiliary metric of Theorem 2.3, induced by the Beltrami coefficient  $\mu$ . Algorithm 1 approximates the auxiliary metric on a triangular mesh [24]. The discrete surface Ricci flow algorithm takes the Riemannian metric as input. Here we use the auxiliary metric to replace the original induced Euclidean metric of the surface, then computing a quasiconformal mapping becomes computing a conformal mapping.

---

### Algorithm 1 Auxiliary Metric

---

**Input:** Triangular mesh  $M = (V, E, F)$  with conformal parameterization  $z : V \rightarrow \mathbb{C}$ , and discrete Beltrami coefficient  $\mu : V \rightarrow \mathbb{C}$  defined on the conformal structure.

**Output:** Discrete auxiliary metric  $\tilde{l}_{ij}$  for all edges  $[v_i, v_j] \in E$ .

- 1: **for all** edge  $[v_i, v_j] \in E$  **do**
  - 2:   Compute the edge length  $l_{ij}$  using the induced Euclidean metric.
  - 3:   Compute the derivative of conformal coordinates on  $[v_i, v_j]$ ,  $dz_{ij} \leftarrow z(v_j) - z(v_i)$ ,
  - 4:   Compute the Beltrami coefficient on  $[v_i, v_j]$ ,  $\mu_{ij} \leftarrow \frac{1}{2}(\mu(v_i) + \mu(v_j))$ ,
  - 5:   Compute the scalar of metric  $\lambda_{ij} \leftarrow \frac{|dz_{ij} + \mu_{ij} dz_{ij}|}{|dz_{ij}|}$ ,
  - 6:   Compute the new auxiliary metric  $\tilde{l}_{ij} \leftarrow \lambda_{ij} l_{ij}$ .
  - 7: **end for**
- 

## 5. Application and Experiments

The main motivation of this work is to improve the efficiency for 3D feature registration and tracking, which is usually very time consuming. It is desirable to reduce the search range for each feature point on surface. This work gives the upper theoretical bound for the search range (distortion) estimation in terms of two parameters: 1) the boundary difference represented by  $\varepsilon$ ; 2) the geometric difference represented by  $\mu$ . In fast 3D scanning applications, both parameters are small, therefore, the search range is small. This greatly improves the tracking efficiency.

In this section, we verify the distortion theorems and evaluate the performance for dynamic feature registration and tracking application by running experiments on 3D human facial scans with dynamic expressions and inconsistent boundaries. For human facial surfaces, geometric difference  $\mu$  includes both human expression difference and subject difference. If we fix the subject and change the expression, then the physical real mapping between the facial surfaces can be fully recovered by its local angle distortion  $\mu$ ; if we change the subject, then the best matching between two faces also gives the  $\mu$ . In theory,  $\mu$  encodes the full information of the mapping; if one knows  $\mu$ , then the original

mapping can be fully reconstructed. In our applications, we only need to know the norm  $\|\mu\|_\infty$ . For simplicity, we use the facial scans from the same subject in each experiment.

**Experimental Design.** *First*, we design the following experiments to verify the theoretical results:

1. Static surface with boundary variations in Section 5.1. In this case, the Beltrami coefficient  $\mu$  is zero,  $\varepsilon_2$  is always zero, and all the distortions are caused by  $\varepsilon_1$ .
2. Dynamic surface with fixed boundary in Section 5.2. In this case, the Beltrami coefficient  $\mu$  is non-zero, and both  $\varepsilon_1$  and  $\varepsilon_2$  are zeros.
3. Dynamic surface with inconsistent boundaries in Section 5.3. In this case, the Beltrami coefficient  $\mu$  is non-zero, and both  $\varepsilon_1$  and  $\varepsilon_2$  are also non-zeros.

*Then*, we apply the distortion upper bounds for feature registration using the boundary variation and non-isometric deformation parameters obtained from our experiments.

### 5.1. Static Surface with Boundary Variation

Figure 3 shows the input face surface (a), which is conformally mapped to the planar unit disk (b). Then we automatically compute 9 loops  $\{\Gamma_k\}$  around the boundary,  $\Gamma_9 \subset \Gamma_8 \cdots \subset \Gamma_1 \subset \Gamma_0 = \partial S_0$ , as shown in (c). Then at step  $k$ , we remove the region outside  $\Gamma_k$  and get a surface  $S_k$ . We conformally map all  $S_k$ ’s to the unit disk with normalization condition,  $\phi_k : S_k \rightarrow \mathbb{D}$ . The normalization is performed as follows: we locate the nose tip and eye corners using the method of [20], and apply a Möbius transformation to map the nose tip to the origin and make the middle point between two eye corners stay in the imaginary axis.

We compute all the boundary points  $z_j \in \Gamma_k$  and measure

$$1) \max ||\phi_k(z_j)| - |\phi_0(z_j)||, \quad 2) \max |arg\phi_k(z_j) - arg\phi_0(z_j)|.$$

The measurements of all the boundary points on conformal mappings are plotted in (d), which is consistent with the distortion estimation theorem on boundary containment (see Theorem 3.1). In addition, Figure 4 illustrates the conformal mappings in the top row, and shows the deformation vector fields  $\phi_k(z_j) - \phi_0(z_j)$  of a set of feature points  $z_j \in S_k$  in the bottom row. The measurement of the above two terms for the interior feature points satisfy Theorem 3.1 as well.

### 5.2. Dynamic Surfaces with Fixed Boundary

In this set of experiments, we ensure the consistency of the surface boundaries, and only change the Beltrami coefficients  $\mu$ , namely, the angle distortion. We conducted two experiments to verify Theorem 3.3, one is on synthetic data, and the other is on captured dynamic raw scans.

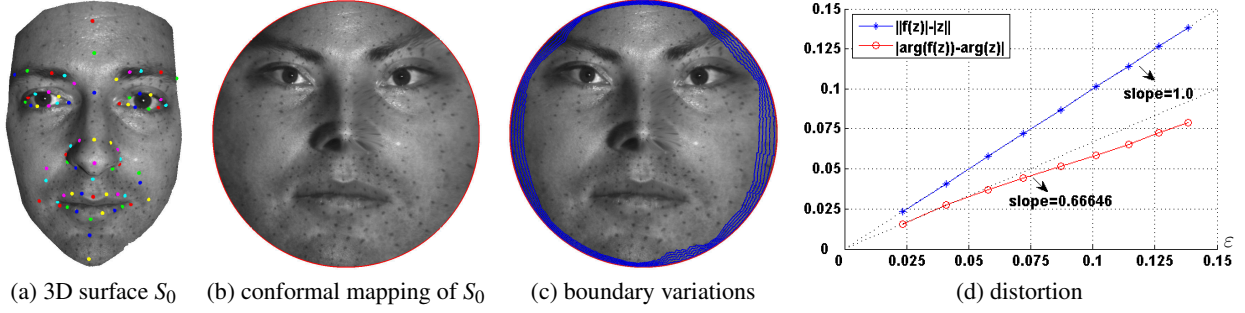


Figure 3. Conformal mappings of a 3D human facial surface with boundary variations. The original boundary of surface (a) is mapped to the red circle on the unit disk (b). The blue loops (c) shows the boundaries, which surround different sizes of areas. (d) plots the distortion of conformal mapping with respect to boundary deviation  $\epsilon$ . The x-axis is the maximal Hausdorff distance between the original boundary and the current boundary. The y-axis is the maximal magnitude/argument distortion. The samples are connected linearly in the plot.

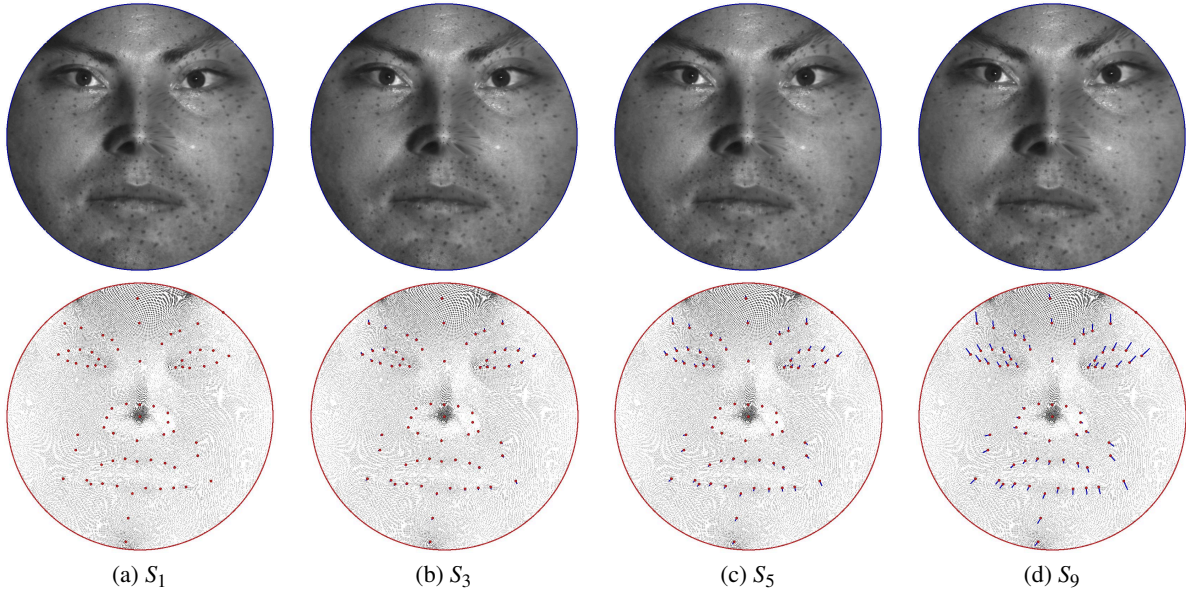


Figure 4. Conformal mapping changes when the boundary varies. The upper row displays the conformal mappings for  $S_1, S_3, S_5, S_9$ ; the bottom row illustrates the deformation vector fields of feature points plotted on the original conformal mapping (see Fig. 3(b)).

**Synthesized Face.** We use a male face surface in Fig. 5(a) and design a one parameter family of deformations  $f_t : \mathbb{D} \rightarrow \mathbb{D}$ , controlled by Beltrami coefficient  $\mu_t, t \in [0, 0.55]$ . First, we conformally map the face surface to the unit disk (b). For each  $z \in \mathbb{D}$ , we set  $\mu_t(z) = tz$ , then solve the Beltrami equation

$$\frac{\partial f_t(z)}{\partial \bar{z}} = \mu_t(z) \frac{\partial f_t(z)}{\partial z},$$

using the algorithm in Section 4.2 to get the quasiconformal mappings as shown in (c-d). We measure the distortions  $\max_{z \in \mathbb{D}} |f_t(z) - z|$ . The distortion curve is plotted in (e), which is consistent with the distortion estimation theorem on non-isometric deformation (see Theorem 3.3).

**Real Scans.** As shown in Fig. 6, we captured a female face expression sequence  $\{S_0, S_1, \dots, S_n\}$  from frame (a)

to frame (b) with controlled consistent boundary condition. We track the face sequence using the algorithm in [24], then compute the Beltrami coefficients for each  $S_k$  using  $S_0$  as the reference surface,  $f_k : S_0 \rightarrow S_k$ , and measure the distortion  $\max_{z \in \mathbb{D}} |f_k(z) - z|$ . The distortion curve with respect to  $\|\mu_k\|_\infty$  is plotted in (e), which verifies Theorem 3.3.

### 5.3. Dynamic Surfaces with Inconsistent Boundary

We capture the dynamic facial surface sequence  $\{S_k\}$  with both expression and pose changes (scanning speed is 30 fps [21]), as shown in Fig. 7(a-b). The facial surface sequence obtained includes both inconsistent boundaries and non-isometric expression deformations (the boundary changes are caused by head rotation, and human facial expressions are non-isometric [23]). We then compute the normalized conformal mappings  $\phi_k : S_k \rightarrow \mathbb{D}$  as described

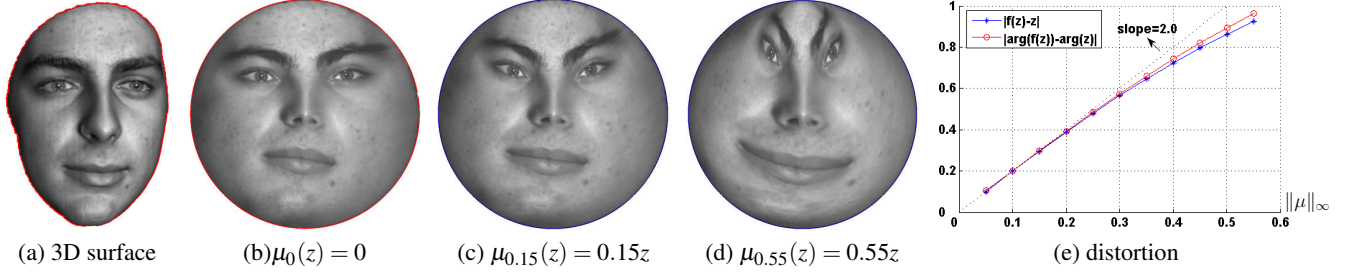


Figure 5. Quasiconformal mappings between a human face surface and a unit disk with varying  $\mu$ .  $\mu_t(z) = tz, z \in \mathbb{D}$ ; and thus  $\|\mu_t(z)\|_\infty = t$ .

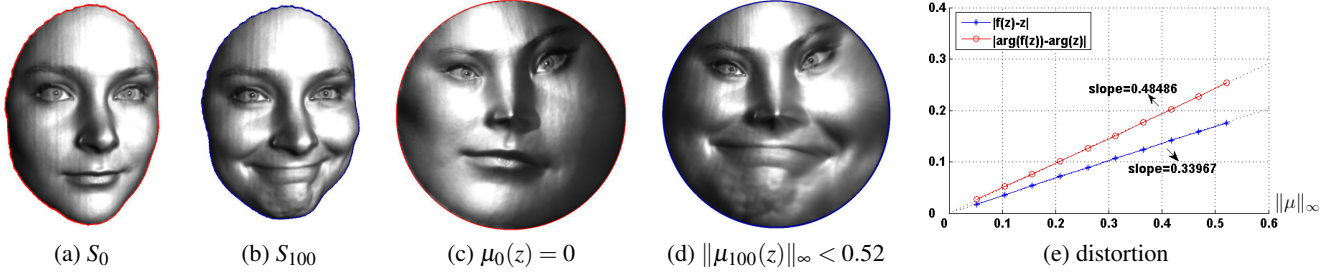


Figure 6. Conformal mappings for a human facial expression sequence  $\{S_k\}$ .  $\mu_k$  is computed from the deformation of  $S_k$  from  $S_0$ .

in Section 5.1. The parameters for Beltrami coefficient  $\mu$  and boundary variation  $\varepsilon$  can be measured on these data. The upper bounds of  $|\mu_k|$ 's and  $\varepsilon_k$ 's between two consecutive frames is less than 0.0025 and 0.0157, respectively.

Based on Theorems 3.1, 3.2, and 3.3, for each point  $z_j \in S_1$ , the range for the corresponding point on  $S_2$ , denoted as  $D_j$ , is constructed as the Minkowski sum of  $\tilde{D}_j$  and a small disk  $d := \{z|z| < 13K\}$ ,  $D_j := \tilde{D}_j + d$ , where

$$\tilde{D}_j := \begin{cases} \{z|z_j| - 2\varepsilon < |z| < |z_j| + 2\varepsilon\} \cap \\ \{z|\arg(z_j) - 2\varepsilon < \arg(z) < \arg(z_j) + 2\varepsilon\}, \end{cases}$$

and Minkowski sum is defined as  $A + B = \{a + b|a \in A, b \in B\}$ . The candidate points corresponding to  $z_j$  must be in  $D_j$ . In practice, the computation of Minkowski sum for non-convex shapes is quadratic and thus expensive, so we use a bounding circle of  $D_j$  as the search range.

We apply the theoretical results to improve the efficiency of feature registration. The sparse feature points on face  $S_k$  are computed first [23]; the generated correspondences are used as ground truth for evaluating the registration accuracy of our feature registration method. Figure 7 demonstrates the feature registration result. Frames (a) and (b) show two facial scans, with big boundary change and a non-isometric expression change, (c) shows the search range for all feature points on the source surface, and (d) shows the displacements of the matched feature points. The surfaces are mapped to a unit disk, and the search radius is selected as 0.24 from the above computation of  $D_j$ . The matching results are completely correct. By using the proposed

distortion estimation, the efficiency for matching has been improved by 5 times, compared with a conformal mapping based registration method using heuristic search range [27].

**Discussion.** For the applications in the same category, the previous results can be used to learn the norm bound of Beltrami coefficient and guide the feature matching for new experiments. So in practice, the norm bound can be treated as a prior. For dynamic facial surfaces with expressions, if the scanning speed is fast, then the norm bound is small; if face expression matching has been done many times, then the norm bound can be learned. Accurate norm bound is unnecessary for many applications. A rough bound can be quite useful already. It is unnecessary to compute a registration. What we need is just the upper bound of the norm.

To the best of our knowledge, till today, this is the only work which gives the distortion estimations of conformal mappings with respect to the variation of boundary and the norm bound of Beltrami coefficient, along with rigorous mathematical proofs. We have tested a broader range of examples on 4 facial sequences with various expression and pose changes (each sequence has 400 frames) and sampled totally 200 pairs of surfaces for computing the distortions of conformal mappings; the experimental results validate the theoretical results.

## 6. Conclusion

The accuracy and stability of surface registration based on conformal mapping method depends on the boundary consistency and the non-isometric deformation. In this

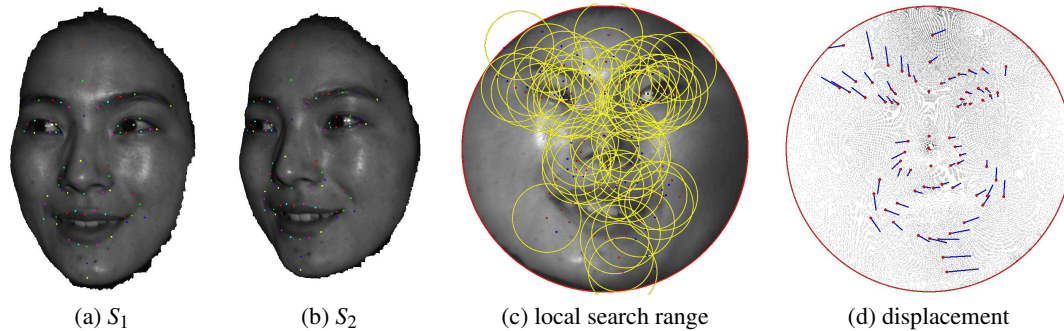


Figure 7. Conformal mapping changes when both the boundary and expression vary. (a) and (b) are two facial surfaces with pose change and dynamic expressions, therefore with different boundaries; feature points are labeled correspondingly. (c) shows the search range for each feature point of (a), where the red and blue dots denote the feature points of (a) and (b), respectively; the yellow circle illustrates the search range for each feature point of (a) on conformal mapping domain (a unit disk) with the search radius 0.24. (d) shows the deformation vector fields of the matched feature points.

work, we estimate the distortions of conformal mappings theoretically and experimentally. We quantify the distortions of conformal mappings caused by both boundary variation and non-isometric deformations. The main theorems claim that the distortions are linear functions of the upper bound of the boundary variation and non-isometric deformation parameters. Furthermore, we present a feature registration algorithm which searches the corresponding features within the range given by the distortion estimation, which improves the efficiency and accuracy of registration.

In future work, we will further improve the bounds of the distortion estimation, and explore further surface tracking algorithm utilizing the theoretical results of this work.

## References

- [1] L. Ahlfors. *Lectures in Quasiconformal Mappings*. Van Nostrand Reinhold, New York, 1966. 2, 3, 4
- [2] P. J. Besl and N. D. McKay. A method for registration of 3-D shapes. *IEEE TPAMI*, 14(2):239–256, 1992. 1
- [3] A. M. Bronstein, M. M. Bronstein, and R. Kimmel. Generalized multidimensional scaling: A framework for isometry-invariant partial surface matching. In *Proceedings of National Academy of Science*, pages 1168–1172, 2006. 1
- [4] R. Campbell and P. Flynn. A survey of free-form object representation and recognition techniques. *Computer Vision and Image Understanding*, 81:166–210, 2001. 1
- [5] B. Chow. The Ricci flow on the 2-sphere. *J. Differential Geom.*, 33(2):325–334, 1991. 3
- [6] M. Feiszli and D. Mumford. Shape representation via conformal mapping. In *Proc. SPIE 6498, Computational Imaging V*, 2007. 1
- [7] A. Frome, D. Huber, R. Kolluri, T. Bulow, and J. Malik. Recognizing objects in range data using regional point descriptors. In *ECCV*, volume III, pages 224–237, 2004. 1
- [8] T. Funkhouser, P. Min, M. Kazhdan, J. Chen, A. Halderman, D. Dobkin, and D. Jacobs. A search engine for 3D models. *ACM TOG*, 22:83–105, 2003. 1
- [9] J. Garnett and D. Marshall. *Harmonic Measure*. New Mathematical Monographs. Cambridge University Press, 2008. 3
- [10] R. S. Hamilton. The Ricci flow on surfaces. *Mathematics and General Relativity*, 71:237–262, 1988. 3
- [11] D. Huber, A. Kapuria, R. Donamukkala, and M. Hebert. Parts-based 3D object classification. In *IEEE CVPR*, 2004. 1
- [12] Y. Lipman. Conformal Wasserstein distances: Comparing surfaces in polynomial time. In *arXiv:1103.4408*, 2011. 1
- [13] L. M. Lui, T. W. Wong, P. M. Thompson, T. F. Chan, X. Gu, and S.-T. Yau. Compression of surface registrations using Beltrami coefficient. In *IEEE CVPR*, 2010. 1
- [14] L. M. Lui, T. W. Wong, W. Zeng, X. Gu, P. M. Thompson, T. F. Chan, and S.-T. Yau. Optimization of surface registrations using beltrami holomorphic flow. *Journal of Scientific Computing (JSC)*, 50(3):557–585, 2012. 1
- [15] R. Osada, T. Funkhouser, B. Chazelle, and D. Dobkin. Shape distributions. *ACM TOG*, 21:807–832, 2002. 1
- [16] S. Ruiz-Correa, L. Shapiro, and M. Meila. A new paradigm for recognizing 3D object shapes from range data. In *IEEE ICCV*. 1
- [17] E. Sharon and D. Mumford. 2D-shape analysis using conformal mapping. *IJCV*, 70:55–75, October 2006. 1
- [18] J. Starck and A. Hilton. Correspondence labelling for wide-timeframe free-form surface matching. In *IEEE ICCV*, 2007. 1
- [19] Y. Sun and M. Abidi. Surface matching by 3D point’s fingerprint. In *IEEE ICCV*, volume II, pages 263–269. 1
- [20] P. Szeptycki, M. Ardabilian, and L. Chen. A coarse-to-fine curvature analysis-based rotation invariant 3d face landmarking. In *IEEE International Conference on Biometrics: Theory, Applications and Systems*. 5
- [21] Y. Wang, M. Gupta, S. Zhang, S. Wang, X. Gu, D. Samaras, and P. Huang. High resolution tracking of non-rigid motion of densely sampled 3D data using harmonic maps. *IJCV*, 76(3):283–300, 2008. 2, 6
- [22] J. Wyngaerd, L. Gool, R. Koch, and M. Proesmans. Invariant-based registration of surface patches. In *IEEE ICCV*. 1
- [23] W. Zeng and X. Gu. 3D dynamics analysis in Teichmüller space. In *IEEE ICCV Workshop on Dynamic Shape Capture and Analysis Recognition (4DMOD’11)*, 2011. 6, 7
- [24] W. Zeng and X. Gu. Registration for 3D surfaces with large deformations using quasi-conformal curvature flow. In *IEEE CVPR*, 2011. 1, 5, 6
- [25] W. Zeng, D. Samaras, and X. D. Gu. Ricci flow for 3D shape analysis. *IEEE TPAMI*, 32(4):662–677, 2010. 1, 5
- [26] W. Zeng, Y. Zeng, Y. Wang, X. T. Yin, X. Gu, and D. Samaras. 3D non-rigid surface matching and registration based on holomorphic differentials. In *ECCV*, 2008. 1
- [27] Y. Zeng, C. Wang, Y. Wang, X. Gu, D. Samaras, and N. Paragios. Dense non-rigid surface registration using high-order graph matching. In *IEEE CVPR*, 2010. 1, 7